Biological Psychiatry: CNNI

Archival Report

Magnetic Resonance Imaging–Derived Markers of Acute and Chronic Inflammatory Processes in the Ventral Tegmental Area Associated With Depression

Sarah Khalife, Steffen Bollmann, Andrew Zalesky, and Lena K.L. Oestreich

ABSTRACT

BACKGROUND: Depression is a leading cause of disability worldwide, with inflammation increasingly recognized as a contributing factor. Inflammatory processes can disrupt the brain's reward circuitry, particularly the ventral tegmental area (VTA), which is central to dopamine-mediated motivation and reward. This study investigates whether magnetic resonance imaging–derived markers sensitive to neuroinflammation and microstructure in the VTA are associated with depression diagnosis and symptom severity.

METHODS: We analyzed diffusion-weighted imaging and quantitative susceptibility mapping data from 32,495 UK Biobank participants, including 3807 individuals with ICD-10–diagnosed major depressive disorder (MDD). Metrics sensitive to neuroinflammation (free water [FW], isotropic volume fraction [ISOVF], magnetic susceptibility) and microstructure (intracellular volume fraction [ICVF], orientation dispersion index [ODI], volume) were extracted from the VTA. Group differences between the MDD group and healthy control (HC) group matched on body mass index, sex, and age were assessed using analysis of variance. Linear regression was used to predict acute symptom severity based on Recent Depressive Symptoms scores.

RESULTS: Participants with an MDD diagnosis had significantly higher FW ($p < .001$) and ISOVF ($p = .001$) compared with HCs, indicating increased extracellular processes such as inflammation in the VTA. Lower ISOVF ($\beta = -0.28$, $p = .033$) and higher ICVF ($\beta = 0.29$, $p = .017$) and ODI ($\beta = 0.4$, $p = .007$) were associated with higher depression severity, independent of depressive diagnosis history.

CONCLUSIONS: Our findings reveal distinct patterns of VTA microstructural changes associated with major depression history versus acute depressive symptom severity, suggesting different underlying pathophysiological mechanisms. Distinct patterns of neuroinflammation may differentiate acute from chronic depression, informing targeted interventions.

https://doi.org/10.1016/j.bpsc.2025.09.003

According to the World Health Organization, depression affects approximately 300 million individuals worldwide, making it a leading cause of disability (1). Depression is a complex, multifactorial disorder, with growing evidence suggesting that inflammation plays a crucial role in its pathophysiology, contributing to both its onset and progression (2). Studies report that individuals with depression often exhibit inflammatory markers and cytokines in their cerebrospinal fluid and blood, suggesting the activation of microglia and astrocytes (see Figure 1) (3). These inflammatory responses can be triggered by various environmental factors, prolonged stress, infections, neurological conditions, and autoimmune diseases, among others (4,5). Chronic inflammation may lead to oxidative and nitrosative stress, causing neurotoxicity and neuronal damage, both of which have been linked to depression (6).

Inflammation disrupts the brain's reward network, which is central to regulating motivation and pleasure (7). Anhedonia and lack of motivation, hallmark symptoms of depression, may be linked to the impact of inflammatory cytokines on mesolimbic dopamine signaling (8). Previous research suggests that inflammatory processes can disrupt the synthesis, release, and reuptake of dopamine, potentially reflecting an adaptive mechanism that prioritizes energy conservation over reward-seeking behaviors during inflammatory states (9). This notion is further supported by animal models demonstrating that inflammation reduces reward-seeking behaviors (10,11).

At the center of the reward network is the ventral tegmental area (VTA), a rich dopaminergic region that plays a critical role in regulating mood, motivation, and reward (12). The VTA is susceptible to ischemia and inflammation, which can lead to neuronal dysfunction in this region (13). Although previous studies have reported decreased VTA activation in depression, microstructural changes in the VTA remain underexplored, likely due to its small, complex structure (14).

ISSN: 2451-9022

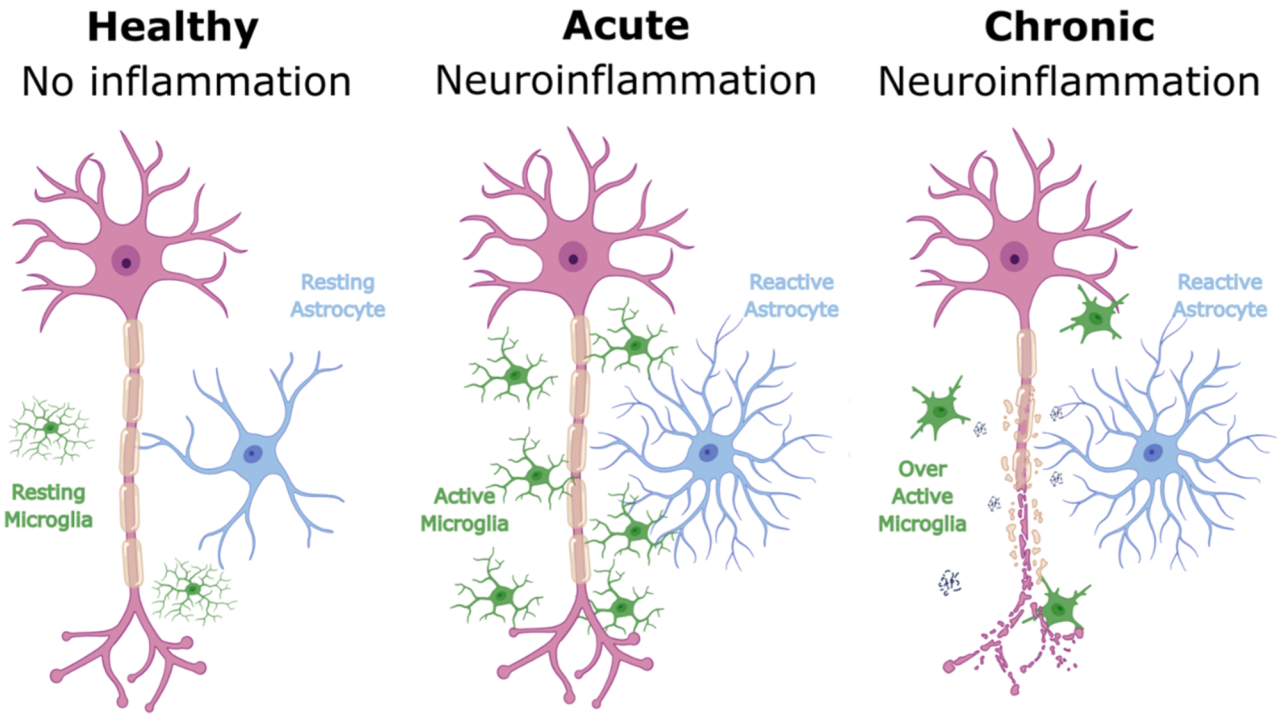

Figure 1. Cellular changes in response to varying degrees of inflammation. The figure illustrates the progression of neuroinflammation from a healthy state to acute and chronic inflammation. In the absence of inflammation, microglia (in green) exhibit a resting morphology with fine, branched processes, and astrocytes (in blue) maintain their characteristic star-shaped structure. During acute neuroinflammation, microglia become activated, adopting an ameboid shape, while astrocytes display hypertrophy, indicating reactivity. In chronic neuroinflammation, sustained elevated cytokine levels cause prolonged activation in both cell types; microglia become overactive, while astrocytes remain reactive. This results in cellular toxicity and potential neurodegeneration, characterized by increased iron deposition and myelin sheath breakdown.

However, recent advancements in neuroimaging, such as high-resolution parcellation atlases, now enable more precise VTA mapping (15).

Several neuroimaging studies have investigated relationships between inflammation and depression, using diverse imaging biomarkers. For example, positron emission tomography (PET) studies have revealed increased radiotracer uptake by microglia in participants with depression, indicating heightened inflammation (16). While the magnetic resonance imaging (MRI)–based technique quantitative susceptibility mapping (QSM) does not directly measure inflammation, it quantifies brain iron accumulation, which may reflect secondary effects of chronic neuroinflammatory processes, such as oxidative stress and prolonged microglial activation (17). QSM is sensitive to tissue magnetic susceptibility, particularly from paramagnetic substances such as iron, as well as diamagnetic components such as calcium and myelin (18). Therefore, abnormal iron distribution observed in depression and other psychiatric disorders (19,20) may provide indirect insights into inflammatory mechanisms over time. Diffusion-weighted imaging (DWI) has similarly revealed inflammation-related microstructural changes (21) and elevated free water (FW) in the extracellular space, commonly associated with inflammatory processes (22). For example, patients with poststroke depression exhibit elevated FW in reward-related regions such as the amygdala and hippocampus (23,24).

In this study, we utilize QSM and DWI to noninvasively examine whether putative markers sensitive to inflammation, as well as microstructural markers that may be altered as a secondary consequence of inflammation, are associated with depression in the VTA. Given the established relationship between inflammation, dopaminergic dysfunction, and depression, as well as the VTA's central role in reward circuitry, we hypothesized that individuals with a history of major depressive disorder (MDD) would exhibit significantly higher levels of QSM- and DWI-derived markers in the VTA compared with matched healthy control (HC) participants. Furthermore, based on the transient nature of inflammation, we hypothesized that acute depression severity would be predicted by MRI markers sensitive to both inflammation and microstructural changes in the VTA irrespective of diagnostic depression history.

METHODS AND MATERIALS

Participants

The UK Biobank (UKB) is a large-scale, prospective epidemiological cohort study comprising approximately 500,000 participants recruited from the general UK population (25). Here, we utilized a subsample of the UKB for whom DWI, QSM, and T1-weighted MRIs of brain anatomy were acquired (n = 46,703). Participants with intellectual disabilities, psychotic or bipolar disorders, and a history of head injury or

neurological conditions were excluded due to their known impact on brain structure (see Table S1 for a detailed variable list). We did not exclude or control for immunometabolic or inflammatory comorbidities due to limited inflammatory data in the UKB at the time of scanning and to maintain the generalizability of findings to real-world clinical populations. Participants with missing data or outliers (>3 SDs from the mean) were excluded, yielding a final sample of 32,495. Ethical approval was granted by the UKB (11/NW/0382; Application No. 100773) and ratified by the University of Queensland (2023/HE000221).

Depression Measures

Of our total sample, 3807 had a history of MDD, based on ICD-10 diagnosis (UKB field ID: 41270). To compare individuals with and without a history of depression, we matched a subset of participants on body mass index (BMI), age, and sex. Descriptive statistics for both groups are presented in Table 1.

To address the possibility that an ICD-10 diagnosis may not reflect current depressive state (some diagnoses were established years before the imaging assessment), we used the Recent Depressive Symptoms (RDS) questionnaire to quantify acute depressive symptoms on the imaging day. The RDS includes 4 items (depressed mood, unenthusiasm/disinterest, tenseness/restlessness, tiredness/lethargy) assessed over the previous 2 weeks, rated on a 4-point Likert scale (1 = not at all, 4 = nearly every day), yielding a total score of 4 to 16 (UKB field IDs: 2050, 2060, 2070, 2080). Higher scores indicate more frequent and severe depressive symptoms, with scores ≥13 representing individuals with particularly high symptom severity. The RDS has been validated against other depression scales, including the Patient Health Questionnaire-9 (26).

Imaging Acquisition and Processing

DW, susceptibility-weighted, and T1-weighted MR images were acquired by the UKB at several sites on a 3T Siemens Skyra scanner with a 32-channel radio frequency receiver head coil, using a standardized acquisition protocol (27).

T1-weighted (1 mm isotropic) and DW (2 mm isotropic) images were acquired using magnetization-prepared rapid acquisition gradient-echo (MPRAGE) and multiband echo-planar imaging sequences, respectively (27). DWI used a multishell approach (b = 1000 and 2000 s/mm^2 with 50 directions per shell, 5 b = 0 s/mm^2, and 1 reverse-phase encoded b = 0 s/mm^2). Preprocessing included gradient distortion, slice outlier, head motion, and eddy current corrections (27). Further details on the preprocessing pipeline can be found in the Supplement. FW-corrected tensor maps were derived from preprocessed DWI data (28), and neurite orientation dispersion and density imaging (NODDI) was estimated by the UKB using Accelerated Microstructure Imaging via Convex Optimization (AMICO) (29,30). NODDI measures included isotropic volume fraction (ISOVF), intracellular volume fraction (ICVF), and orientation dispersion index (ODI). QSM images from susceptibility-weighted imaging were minimally preprocessed by the UKB (27) and minimum-maximum normalized (0–1) for comparison.

Neuroimaging analyses were conducted on the University of Queensland's high-performance computer Bunya (31), utilizing Neurodesk (32). The VTA was delineated with the Levinson-Bari Limbic Brainstem Atlas (15), with T1 images coregistered to DWI using advanced normalization tools (ANTs) (33), followed by Montreal Neurological Institute (MNI)-to-T1 registration and transformation to DWI space (34) (see Figure 2). QSM images were similarly coregistered to DWI participant space. To validate the accuracy of the atlas-derived VTA mask, we manually segmented the VTA in an independent 7T dataset using high-resolution T1 and QSM images. The atlas was coregistered to each participant's T1 image in subject space using the same protocol as in the main analysis, and spatial overlap was quantified using the dilated Dice similarity coefficient. Full details and results, which validated that atlas-based VTA masks were well localized, are described in the Supplement.

We extracted FW, ISOVF, and magnetic susceptibility from the VTA, as these metrics have previously been reported to be associated with neuroinflammation (35–37). While both FW

Table 1. Demographic and VTA MRI Metrics in HC Participants and Individuals With ICD-10 MDD History

Variable	Total, N = 32,495	HCs, n = 3807	MDD History, n = 3807	p Value
Sex, Female	16,806 (51.7%)	2435 (64%)	2431 (63.9%)	–
Age, Years	63.9 (7.7)	62.4 (7.6)	62.5 (7.6)	.788
BMI	26.2 (3.9)	26.9 (4.2)	26.9 (4.2)	.740
RDS Score	5.2 (1.7)	5.1 (1.6)	6.5 (2.6)	<.001*
MRI-Derived Metrics				
ICVF	0.533 (0.074)	0.531 (0.073)	0.527 (0.072)	.044**
ODI	0.295 (0.073)	0.294 (0.073)	0.298 (0.073)	.025**
ISOVF	0.374 (0.114)	0.366 (0.115)	0.375 (0.115)	.001***
FW	0.456 (0.101)	0.451 (0.102)	0.459 (0.103)	.001*
Magnetic susceptibility	0.395 (0.072)	0.393 (0.071)	0.394 (0.072)	.457
Volume ratio	7.025×10^{-4} (1.98×10^{-4})	7.135×10^{-4} (2.057×10^{-4})	7.076×10^{-4} (2.006×10^{-4})	.201

Values are presented as n (%) or mean (SD). Magnetic resonance imaging (MRI) metrics from the ventral tegmental area (VTA) provide insights into microstructural and inflammatory characteristics. p Values indicate the significance of differences between healthy control (HC) and major depressive disorder (MDD) history groups.

*$p < .05$, **$p < .01$, ***$p < .001$.

BMI, body mass index; FW, free water; ICVF, intracellular volume fraction; ISOVF, isotropic volume fraction; ODI, orientation dispersion index; RDS, Recent Depressive Symptoms.

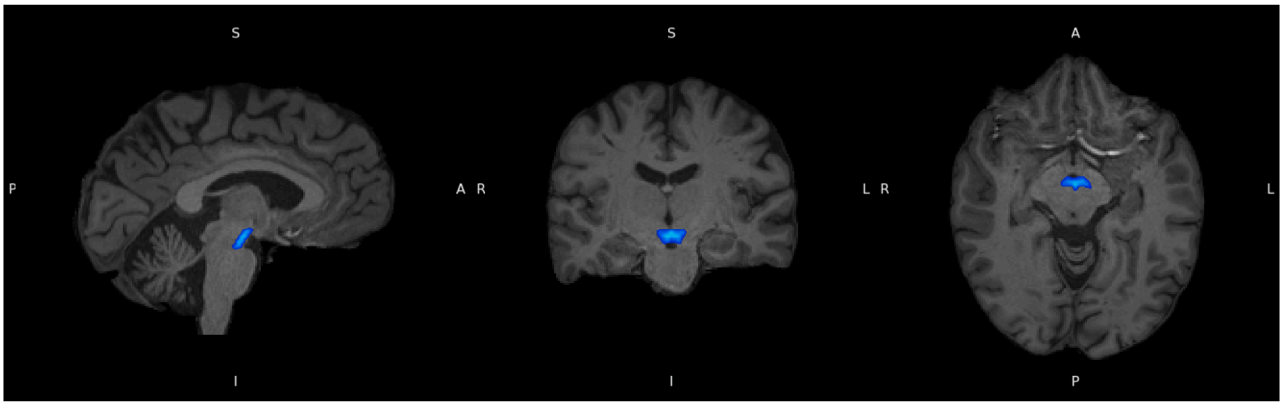

Figure 2. Ventral tegmental area (in blue), delineated using the Levinson-Bari Limbic Brainstem Atlas, displayed on coregistered participant T1 images. A, anterior; I, inferior; L, left; P, posterior; R, right; S, superior.

and ISOVF measure free water, ISOVF requires advanced protocols, while FW is more clinically accessible. ICVF and ODI were also extracted to investigate potential microstructural changes associated with acute and prolonged neuroinflammation. VTA volume was adjusted for total intracranial volume to account for individual brain size differences.

While our primary focus was on the VTA, we conducted exploratory analyses in additional regions implicated in MDD, including the orbitofrontal cortex, insula, amygdala, hippocampus, ventral anterior cingulate cortex (ACC), medial prefrontal cortex, posterior cingulate cortex, precuneus, angular gyrus, dorsolateral prefrontal cortex, dorsal ACC, prefrontal cortex, caudate, and nucleus accumbens (38). Full results are presented in Tables S3 to S5.

Statistical Analysis

Group differences on demographic and clinical variables were tested using *t* tests and χ^2 tests. To examine associations between depression diagnosis and MRI-derived VTA metrics (FW, ISOVF, QSM, ICVF, ODI, volume), we conducted one-way analyses of variance (ANOVAs) with group (MDD/HC) as the between-subjects factor. Bonferroni correction was applied, setting the corrected alpha level at 0.0083 (0.05/6 comparisons), and effect sizes were reported as η_p^2. Groups were matched on age, sex, and BMI.

To assess whether VTA MRI metrics predicted current depressive symptom severity, we performed linear regression using MRI markers as predictors and RDS scores as the outcome. VTA volume was not included in the regression models due to concerns about the accuracy of atlas-based volume estimates in small brainstem structures and to avoid introducing additional noise into the analysis. To ensure adequate representation of individuals with high depressive symptom severity, we identified a reference group with RDS scores $\geq$13 (indicative of high symptom severity). Given the limited number of participants in this high-severity reference group ($<$100 participants), we limited the sampling of participants with lower RDS scores to a maximum of 100 participants per RDS score. The selection was pseudorandomized and iterated (50,000 permutations) to closely match age and sex with the high-symptom group. Residual confounding was addressed by controlling for age, age^2, sex, BMI, and the log-transformed duration and number of depression episodes (capped at 100) (Tables S5 and S6). Log transformation was applied to reduce skew and enhance sensitivity to lower-range values. Standardized coefficients were reported for effect size comparison. Multicollinearity was checked using the variance inflation factor (VIF), and correlations among predictors were explored (Figure S2).

RESULTS

Association Between VTA-Derived MRI Markers and MDD Diagnosis

As shown in Table 1, our groups consisted of 64% females, were 62.5 $\pm$ 7.6 years of age, and had a BMI of 26.9 $\pm$ 4.2. No significant differences were found in age, sex, or BMI, but the depression history group had significantly higher RDS scores than the HC group (t_{6327} = 28.3, $p < .001$).

ANOVAs revealed that the MDD group exhibited significantly higher FW ($F_{1,7612}$ = 12.29, $p < .001$, η_p^2 = 0.002) and ISOVF ($F_{1,7612}$ = 10.26, p = .001, η_p^2 = 0.001) compared with the HC group, suggesting increased extracellular inflammation–related processes in the VTA among individuals with a history of depression. The findings of higher ICVF ($F_{1,7612}$ = 4.06, p = .044, $\eta_p^2 = 5.34 \times 10^{-4}$) and ODI ($F_{1,7612}$ = 4.99, p = .025, $\eta_p^2 = 6.56 \times 10^{-4}$) in the MDD group compared with the HC group did not survive Bonferroni correction. No significant group differences were observed for volume ($F_{1,7612}$ = 1.63, p = .2, η_p^2 = 0.0002) or magnetic susceptibility ($F_{1,7612}$ = 0.55, p = .457, $\eta_p^2 = 7.2 \times 10^{-5}$). Group means and distributions are visualized in Figure 3. Across the additional brain regions examined, relative to HC participants, individuals with a history of MDD showed significantly higher ISOVF and FW in several cortical and subcortical areas, including the orbitofrontal cortex, insula, hippocampus, and caudate, indicating that greater extracellular water content and potential microstructural alterations associated with depression extend to these regions.

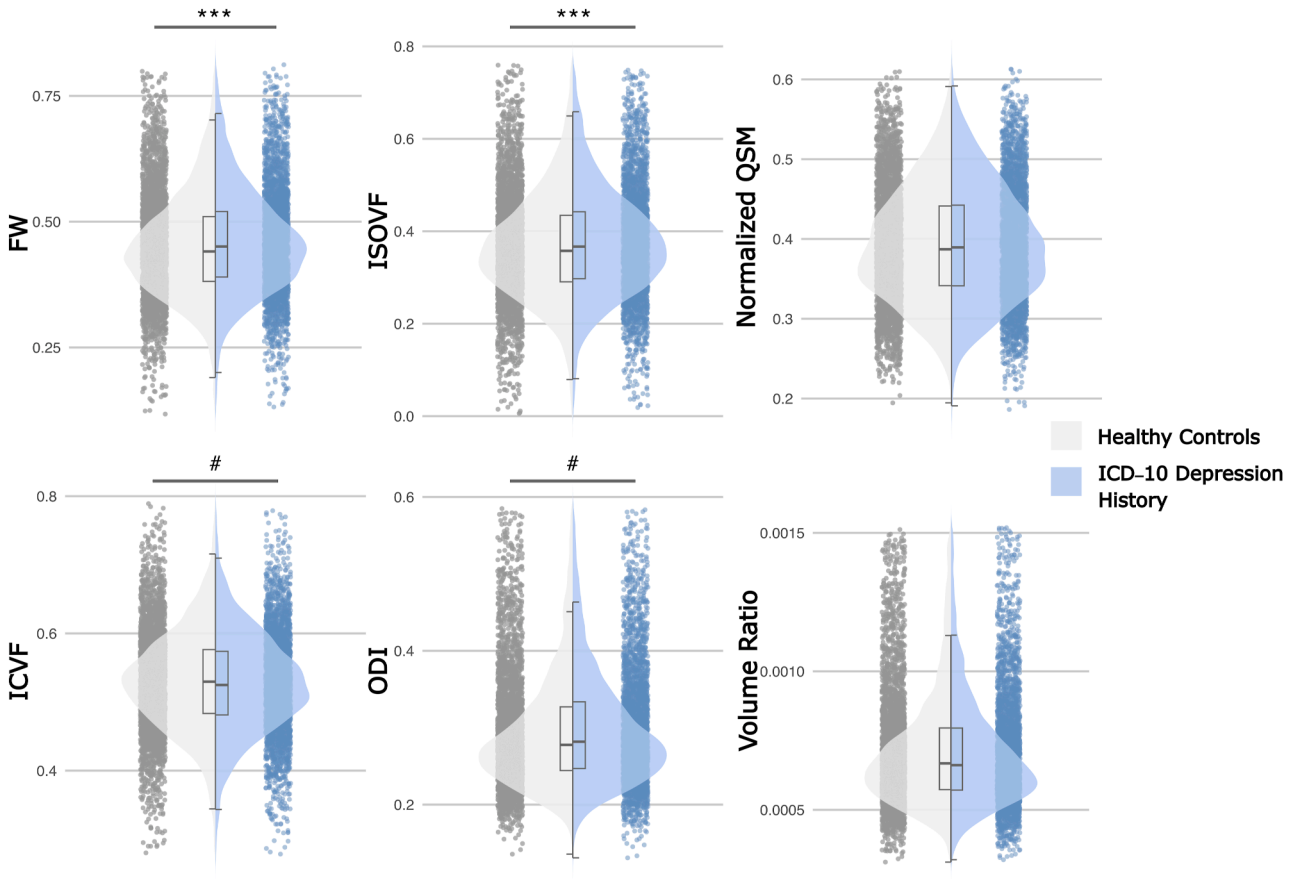

Figure 3. Group comparisons between healthy control participants and individuals with an ICD-10 history of major depressive disorder. *** represents significant group differences that were sustained even after multiple comparison correction (p value $\leq$ .001), and # indicates significant group differences before multiple corrections. Magnetic resonance imaging (MRI) metrics from the ventral tegmental area (VTA), including intracellular volume fraction (ICVF), orientation dispersion index (ODI), isotropic volume fraction (ISOVF), free water (FW), quantitative susceptibility mapping (QSM), and standardized volume ratio.

VTA-Derived MRI Markers as Predictors of Acute Depression Severity

The final subsample included 1151 participants, comprising individuals from the high-symptom reference group (RDS score $\geq$ 13) and the best-matched lower-symptom group (RDS score $<$ 13). Descriptive statistics for the full sample and subgroups are shown in Table 2. The total subsample consisted of 58% females, with a mean age of 60.9 $\pm$ 7.4 years and a BMI of 27.2 $\pm$ 4.4.

FW (VIF = 34.12) and ISOVF (VIF = 33.08) showed high multicollinearity in the regression model, supported by their strong correlation (r = 0.96, $p < .001$), suggesting that they reflect similar processes, allowing them to be used interchangeably. To reduce redundancy and for consistency with other NODDI metrics, FW was excluded and ISOVF retained as a proxy for extracellular inflammation. After excluding FW, ISOVF VIF decreased to 1.82, and all other variables (except age and age^2) had VIFs < 5, indicating that multicollinearity was resolved. See Figure S2 for correlation details.

The linear regression model was significant ($F_{10,1140}$ = 19.73, $p < .001$), explaining 14% of the variance in depression severity (R^2 = 0.148, adjusted R^2 = 0.14). As shown in Figure 4A, the model showed moderate fit with slight overestimation near the center of the distribution. Standardized beta coefficients are presented in Figure 4B. Both ICVF (β = 0.29; p = .017; 95% CI, 0.053 to 0.53) and ODI (β = 0.4; p = .007; 95% CI, 0.11 to 0.7) were positively associated with depressive symptom severity, indicative of an increase in microstructural changes with higher depression severity. Elevated ODI values suggest increased microstructural changes in the extracellular space, while higher ICVF values indicate greater neurite density associated with worsening depression symptoms. ISOVF showed a negative association with depression severity ($\beta = -0.28$; p = .033; 95% CI, -0.53 to -0.02), indicating that decreased NODDI FW was linked to greater symptom severity. In contrast, magnetic susceptibility was not significantly associated with depressive symptom severity.

Sex was a significant predictor of depression severity, with males exhibiting lower depressive symptom severity compared with females ($\beta = -0.4$; $p < .001$; 95% CI, -0.6 to -0.2). Additionally, BMI was positively associated with depressive severity (β = 0.38; $p < .001$; 95% CI, 0.18 to 0.57), suggesting that higher BMI may be linked to increased

Table 2. Demographic and VTA MRI Metrics Across Subgroups With Varying Levels of Recent Depressive Symptoms

Variable	Total Subsample, n = 1151	Best Matched, RDS Score < 13, n = 900	Reference, RDS Score ≥ 13, n = 251
Sex, Female	667 (57.9%)	506 (56.2%)	161 (64.1%)
Age, Years	60.9 (7.4)	61.3 (7.5)	59.5 (6.9)
BMI	27.2 (4.4)	26.9 (4.2)	27.9 (5)
RDS Score	9.4 (3.5)	8 (2.6)	14.4 (1.2)
MRI-Derived Metrics			
ICVF	0.529 (0.074)	0.527 (0.074)	0.533 (0.074)
ODI	0.297 (0.077)	0.297 (0.078)	0.296 (0.076)
ISOVF	0.371 (0.115)	0.375 (0.115)	0.356 (0.115)
FW	0.455 (0.103)	0.459 (0.103)	0.441 (0.104)
Magnetic susceptibility	0.392 (0.07)	0.391 (0.069)	0.394 (0.073)
Volume ratio	7.128×10^{-4} (2.01×10^{-4})	7.125×10^{-4} (2.01×10^{-4})	7.139×10^{-4} (2.016×10^{-4})

Values are presented as n (%) or mean (SD). Main analysis was run on the total subsample.

BMI, body mass index; FW, free water; ICVF, intracellular volume fraction; ISOVF, isotropic volume fraction; MRI, magnetic resonance imaging; ODI, orientation dispersion index; RDS, Recent Depressive Symptoms; VTA, ventral tegmental area.

severity of depressive symptoms. Notably, the number of lifetime depressive episodes ($\beta = 0.58$; $p < .001$; 95% CI, 0.34 to 0.82) and the duration of the longest depressive episode in weeks ($\beta = 0.54$; $p < .001$; 95% CI, 0.30 to 0.78) were also significant predictors, indicating that greater depression chronicity was associated with more severe current symptoms. The covariates age and age^2 were not significantly associated with depressive symptom severity.

DISCUSSION

This study provides novel insights into the neurobiological correlates of depression, revealing a complex relationship between structural and inflammatory markers in the VTA and depressive symptomatology. Our findings demonstrate that individuals with a diagnosis of MDD exhibited significantly higher extracellular FW in the VTA compared with matched HCs, suggesting extraneuronal pathology potentially linked to

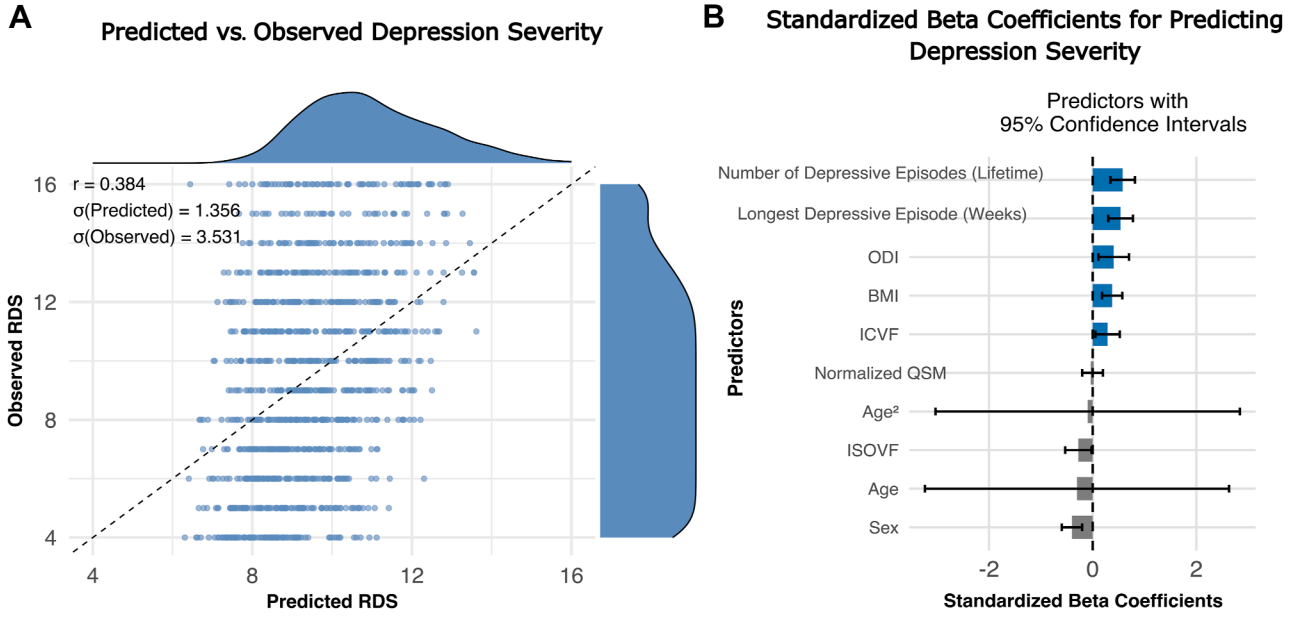

Figure 4. **(A)** Scatter plot depicting the relationship between predicted and observed depression severity scores (Recent Depressive Symptoms [RDS]) derived from the linear regression model. Each point represents an individual participant, with the dashed identity line (y = x) included for reference. The marginal density plots illustrate the distribution of predicted and observed scores. The Pearson correlation coefficient (r), together with the standard deviations of the predicted and observed RDS values, is annotated. **(B)** Standardized beta coefficients from the regression model predicting depression severity. Bars represent the effect size of each predictor, with 95% CIs indicated by error bars. Positive predictors (e.g., orientation dispersion index [ODI], body mass index [BMI], intracellular volume fraction [ICVF]) are shown in blue, while negative predictors are shown in gray. The dashed horizontal line at 0 represents the null effect. Variables are ordered by effect size for clarity. ISOVF, isotropic volume fraction.

inflammatory processes. While these inflammatory markers were elevated, no structural alterations or differences in iron deposition (estimated via QSM) were observed between groups. Notably, MRI markers sensitive to inflammation and structural changes in the VTA predicted acute depressive symptom severity, independent of prior history of MDD diagnosis, with higher ICVF and ODI and lower ISOVF associated with more severe depressive symptoms. In contrast, magnetic susceptibility did not predict symptom severity, reinforcing the absence of chronic inflammation–related effects such as cell damage or iron accumulation.

ISOVF and FW are MRI markers sensitive to neuroinflammation and edema (28,29). Although derived from different diffusion models (3-compartment NODDI for ISOVF and 2-compartment tensor modeling for FW), both quantify freely diffusing water and can reflect extracellular fluid increases associated with inflammatory processes such as vasogenic edema and associated cellular responses (28). Therefore, elevated ISOVF and FW in individuals with a history of MDD are consistent with our prediction that major depression is associated with elevated inflammation markers in the VTA. In contrast, while FW and ISOVF were elevated in individuals with MDD, we observed that acute depression severity in the general population was associated with lower ISOVF. This dissociation suggests these two states of depression—historical diagnosis of major depression versus acute depressive symptoms across the general population—may reflect distinct biological processes and inflammatory states. Yi *et al.* (39) highlighted important distinctions between acute and chronic inflammation, showing that acute neuroinflammation is marked by increased hindered water diffusion due to increases in the number of activated hyperramified microglia, while chronic inflammation is marked by reduced hindered diffusion due to overactivation of microglia, which increases their density. Thus, our findings of lower ISOVF may reflect acute inflammation processes, while the elevated ISOVF and FW may be indicative of chronic inflammatory processes in major depression.

Increased FW is often associated with psychiatric symptom severity and neuroinflammation in psychiatric and neurological disorders (22,40–42), although findings in depression remain mixed. For example, elevated FW has been reported in patients with poststroke depression in reward-related regions (22), suggesting vulnerability of these areas to inflammation. Conversely, Bergamino *et al.* (40) found no FW differences between HCs and unmedicated patients with MDD. Consistent with our findings, Althubaity *et al.* (43) reported reduced ISOVF in the gray matter of individuals with depression, particularly in the ACC of individuals with low peripheral inflammation, although this difference was not statistically significant across the entire depression group. The ACC, like the VTA, has shown decreased functional MRI activation and increased microglial expression in PET studies (44). However, no significant ISOVF differences were found in the prefrontal or insular cortices across inflammation subgroups or overall depressed versus control groups (43). These findings suggest that FW and ISOVF changes may reflect distinct, localized processes, potentially influenced by acute or chronic inflammation associated with depression. Given the reward network's sensitivity to neuroinflammatory processes and its central role in dopamine signaling (9–11), these regions may exhibit differential responses to such changes, with prolonged depressive episodes possibly impacting the VTA's structural integrity in a manner distinct from acute depressive symptoms.

Our results indicate that the VTA is also susceptible to microstructural aberrations possibly linked to inflammation in depression. While ICVF and ODI differences did not survive Bonferroni correction in group comparisons, our regression analysis identified both metrics as independent predictors of depression severity. Elevated ICVF, which is typically interpreted as increased neurite density and intracellular diffusion, has also been associated with glial swelling and microglial reactivity, key features of depression (20,45). Similar increases in ICVF have been reported in the striatum following interferon alpha–induced inflammation (46). Although fatigue (a symptom of depression) increased, no significant rise in depression severity was observed, suggesting that inflammation affects reward circuitry even in the absence of amplifying mood symptoms (46). This may explain the vulnerability of the VTA and striatum to inflammation in depression, which is consistent with our findings of increased ICVF in the VTA, a structure closely linked to the brain's reward system, reinforcing its vulnerability to inflammatory processes and depression. Higher ODI levels in the VTA may reflect microstructural processes in the extracellular space, where microglia modulate immune defense. Yi *et al.* (39) demonstrated that increased ODI correlated with microglial density, further suggesting that microglial activation could be driving these microstructural changes. Similarly, Ota *et al.* (47) reported reduced ODI in the thalamus of individuals with MDD, and postmortem studies found decreased astrocytic markers in the thalamus of deceased individuals with MDD, lending additional support for the involvement of glial cells in depression (48).

Our study found no significant differences in VTA volume between individuals with depression and healthy individuals. This contrasts with findings by Morris *et al.* (49), who reported increased VTA volume linked to alterations in neuromelanin and dopamine activity in individuals with mood disorders. The absence of volumetric differences in our study suggests that the observed microstructural changes, such as higher ICVF and ODI, may occur independently of gross volumetric changes.

Even though QSM is sensitive to the effects of prolonged inflammation, our study found no significant differences in magnetic susceptibility between individuals with major depression and HCs in the VTA; it was also not a predictor of acute depressive severity. This suggests that processes such as iron deposition, demyelination, or cell death, typically associated with chronic inflammation, may not significantly impact VTA structure as hypothesized. However, Yao *et al.* (20) reported higher susceptibility values correlating with current depression severity in the putamen and thalamus. Duan *et al.* (19) found that magnetic susceptibility in the thalamus, hippocampus, and putamen correlated with depression duration rather than current symptom severity, suggesting that microstructural changes accumulate over time. The discrepancy between our VTA findings and previous work in other regions may reflect the distinct cellular architecture and inflammatory vulnerability of different brain areas.

The VTA, primarily composed of dopaminergic neurons and their supporting glial cells, may respond differently to inflammatory processes compared with regions such as the putamen and thalamus, which have different cellular compositions and metabolic demands. While Yao *et al.* (20) and Duan *et al.* (19) demonstrated susceptibility changes in striatal and limbic regions, our findings suggest that the VTA may be more resilient to chronic inflammatory processes that lead to iron accumulation or cellular damage. Instead, the VTA appears to show more dynamic changes in the extracellular space (as indicated by FW measures) that may reflect acute rather than chronic inflammatory states.

While statistically significant, our findings had small effect sizes, reflecting the multifactorial nature of depression. Depression is influenced by numerous factors, including sex, lifestyle factors, genetic predisposition, and metabolic variables such as BMI (50), which explained a substantial portion of the variance in our models. Our findings showed that females were significantly more likely to have higher depressive symptoms, consistent with previous literature indicating a higher prevalence of depression in females, potentially due to factors such as reporting tendencies and hormonal influences (51). BMI was also a positive predictor of depression severity, consistent with studies that have shown obesity to be associated with elevated cytokine levels, reduced physical activity, and heightened depression risk (52,53).

Additionally, depression history and chronicity, as measured by the number and duration of previous depressive episodes, were significant predictors of current symptom severity. This is consistent with previous research showing that recurrent and prolonged episodes are associated with greater functional impairment and an increased risk of future depressive episodes (54). However, we acknowledge that these measures were based on retrospective self-report and did not include precise timing information (e.g., when episodes occurred), which may limit the reliability and interpretability of these findings. These results underscore the complex interplay between neuroinflammation, lifestyle factors, and depressive symptoms, suggesting that future studies should consider these factors in more detail to fully understand the multifactorial nature of depression.

One important limitation of our study is the cross-sectional design, which limits our ability to establish causal relationships between neuroinflammation, VTA microstructural changes, and depression severity. Additionally, while a significant portion of our participants experienced multiple major depressive episodes between their initial ICD-10 depression diagnosis and the time of scanning, the average time since their first diagnosis was approximately 27 $\pm$ 11.15 years prior to the scan. Future longitudinal studies should explore the relationship between recurrent depressive episodes and the interplay of chronic and acute depression on brain structure. Furthermore, while DWI and QSM provide valuable insights into brain structure and inflammation, they are indirect measures. Integrating these methods with more direct biomarkers, such as cerebrospinal fluid cytokine levels or PET imaging, would provide stronger evidence of neuroinflammation's role in depression. Lastly, while the atlas-based registration captures the VTA well, it encompasses small portions of neighboring structures such as the red nucleus and substantia nigra, which is a common limitation when studying such small, anatomically adjacent nuclei. As a result, the diffusion metrics attributed to the VTA may partially reflect signal from these adjacent regions.

Conclusions

Our findings reveal distinct patterns of microstructural changes in the VTA associated with both major depression history and current depressive symptom severity, suggesting different underlying pathophysiological mechanisms. The elevated FW markers observed in individuals with a major depression history, coupled with the relationship between NODDI metrics and current symptom severity, point to dynamic inflammatory processes that may differ between acute and chronic states of depression. While our results support the role of neuroinflammation in depression, the absence of QSM changes suggests that the VTA may be more resilient to chronic inflammatory processes compared with other brain regions. These findings could ultimately inform more targeted therapeutic approaches that consider the distinct biological processes underlying depression.

ACKNOWLEDGMENTS AND DISCLOSURES

LKLO was supported by a National Health and Medical Research Council Investigator Grant (Grant No. 2 007 718), a strategic award from the School Psychology (Division 16), and a start-up fund from the Australian Institute for Bioengineering and Nanotechnology, University of Queensland.

Presented as a poster at the Organization of Human Brain Mapping Annual Conference 2024, Seoul, South Korea, June 25, 2024, and the Organization of Human Brain Mapping Annual Conference 2025, Brisbane, Australia, June 24, 2025.

All the neuroimaging preprocessing and analyses conducted in this study involved the use of publicly available toolboxes and resources. Specifically, the following software tools were used: FreeSurfer (version 7.4.1) (55,56), FSL (version 6.0.7.4) (57,58), FSLeyes (version 1.10.4) (59), MRtrix3 (version 3.0.3) (60), and ANTs (version 2.3.5) (33). For statistical analysis, both ANOVAs and regression analyses were run through R and RStudio (61), using *dplyr*, *ggplot2*, *ggpubr*, *skimr*, *plotly*, *htmlwidgets*, *MatchIt*, *gghalves*, *psych*, *GGally*, *tidyverse*, *car*, *kableExtra*, *officer*, *tcltk*, and *scales* packages and functions (62–77). The FW imaging code, developed by Pasternak *et al.* (28), is not publicly available but can be obtained from the authors upon request. All other code and materials used in this study are available at https://github.com/Psychedelics-Clinical-Neuroimaging-Lab/UKB_VTA_Inflammation_Data_Prep_and_Stat/tree/main. Due to ethical considerations, raw data from the UK Biobank cannot be shared directly.

The authors report no biomedical financial interests or potential conflicts of interest.

ARTICLE INFORMATION

From the School of Psychology, The University of Queensland, Brisbane, Queensland, Australia (SK, LKLO); School of Electrical Engineering and Computer Science, The University of Queensland, Brisbane, Queensland, Australia (SB); Queensland Digital Health Centre, The University of Queensland, Brisbane, Queensland, Australia (SB); Systems Lab, Department of Psychiatry, The University of Melbourne, Melbourne, Victoria, Australia (AZ); Department of Biomedical Engineering, The University of Melbourne, Parkville, Victoria, Australia (AZ); and Australian Institute for Bioengineering and Nanotechnology, The University of Queensland, Brisbane, Queensland, Australia (LKLO).

Address correspondence to Sarah Khalife, B.Sc., at s.khalife@uq.edu.au.

Received Mar 5, 2025; revised Jul 25, 2025; accepted Sep 3, 2025.

Supplementary material cited in this article is available online at https://doi.org/10.1016/j.bpsc.2025.09.003.

REFERENCES

1. World Health Organization: Depression and other common mental disorders: Global health estimates. Geneva, Switzerland: World Health Organization. Available at: https://apps.who.int/iris/handle/10665/254610. Accessed February 1, 2023.
2. Ménard C, Hodes GE, Russo SJ (2016): Pathogenesis of depression: Insights from human and rodent studies. Neuroscience 321:138–162.
3. Raison CL, Capuron L, Miller AH (2006): Cytokines sing the blues: Inflammation and the pathogenesis of depression. Trends Immunol 27:24–31.
4. Banerjee A, Khemka VK, Roy D, Dhar A, Sinha Roy TK, Biswas A, *et al.* (2017): Role of pro-inflammatory cytokines and vitamin D in probable Alzheimer's disease with depression. Aging Dis 8:267–276.
5. Prasad S, Tyagi AK, Aggarwal BB (2016): Detection of inflammatory biomarkers in saliva and urine: Potential in diagnosis, prevention, and treatment for chronic diseases. Exp Biol Med (Maywood) 241:783–799.
6. Somani A, Singh AK, Gupta B, Nagarkoti S, Dalal PK, Dikshit M (2022): Oxidative and nitrosative stress in major depressive disorder: A case control study. Brain Sci 12:144.
7. Felger JC, Li Z, Haroon E, Woolwine BJ, Jung MY, Hu X, Miller AH (2016): Inflammation is associated with decreased functional connectivity within corticostriatal reward circuitry in depression. Mol Psychiatry 21:1358–1365.
8. Felger JC, Treadway MT (2017): Inflammation effects on motivation and motor activity: Role of dopamine. Neuropsychopharmacology 42:216–241.
9. Straub RH (2017): The brain and immune system prompt energy shortage in chronic inflammation and ageing. Nat Rev Rheumatol 13:743–751.
10. Nunes EJ, Randall PA, Estrada A, Epling B, Hart EE, Lee CA, *et al.* (2014): Effort-related motivational effects of the pro-inflammatory cytokine interleukin 1-beta: Studies with the concurrent fixed ratio 5/chow feeding choice task. Psychopharmacology (Berl) 231:727–736.
11. Yohn SE, Arif Y, Haley A, Tripodi G, Baqi Y, Müller CE, *et al.* (2016): Effort-related motivational effects of the pro-inflammatory cytokine interleukin-6: Pharmacological and neurochemical characterization. Psychopharmacology (Berl) 233:3575–3586.
12. Tye KM, Mirzabekov JJ, Warden MR, Ferenczi EA, Tsai HC, Finkelstein J, *et al.* (2013): Dopamine neurons modulate neural encoding and expression of depression-related behaviour. Nature 493:537–541.
13. Pisani A, Bonsi P, Calabresi P (2004): Calcium signaling and neuronal vulnerability to ischemia in the striatum. Cell Calcium 36:277–284.
14. Halliday GM, Törk I (1986): Comparative anatomy of the ventromedial mesencephalic tegmentum in the rat, cat, monkey and human. J Comp Neurol 252:423–445.
15. Levinson S, Miller M, Iftekhar A, Justo M, Arriola D, Wei W, *et al.* (2022): A structural connectivity atlas of limbic brainstem nuclei. Front Neuroimaging 1:1009399.
16. Gritti D, Delvecchio G, Ferro A, Bressi C, Brambilla P (2021): Neuroinflammation in major depressive disorder: A review of PET imaging studies examining the 18-kDa translocator protein. J Affect Disord 292:642–651.
17. Eskreis-Winkler S, Zhang Y, Zhang J, Liu Z, Dimov A, Gupta A, Wang Y (2017): The clinical utility of QSM: Disease diagnosis, medical management, and surgical planning. NMR Biomed 30.
18. Liu C, Wei H, Gong NJ, Cronin M, Dibb R, Decker K (2015): Quantitative susceptibility mapping: Contrast mechanisms and clinical applications. Tomography 1:3–17.
19. Duan X, Xie Y, Zhu X, Chen L, Li F, Feng G, Li L (2022): Quantitative susceptibility mapping of brain iron deposition in patients with recurrent depression. Psychiatry Investig 19:668–675.
20. Yao S, Zhong Y, Xu Y, Qin J, Zhang N, Zhu X, Li Y (2017): Quantitative susceptibility mapping reveals an association between brain iron load and depression severity. Front Hum Neurosci 11:442. [cited Sep 22 2024].
21. Zhang W, Rutlin J, Eisenstein SA, Wang Y, Barch DM, Hershey T, *et al.* (2023): Neuroinflammation in the amygdala is associated with recent depressive symptoms. Biol Psychiatry Cogn Neurosci Neuroimaging 8:967–975.
22. Oestreich LKL, O'Sullivan MJ (2022): Transdiagnostic in vivo magnetic resonance imaging markers of neuroinflammation. Biol Psychiatry Cogn Neurosci Neuroimaging 7:638–658.
23. Green C, Shen X, Stevenson AJ, Conole ELS, Harris MA, Barbu MC, *et al.* (2021): Structural brain correlates of serum and epigenetic markers of inflammation in major depressive disorder. Brain Behav Immun 92:39–48.
24. Oestreich LKL, Wright P, O'Sullivan MJ (2020): Microstructural changes in the reward system are associated with post-stroke depression. Neuroimage Clin 28:102360.
25. Allen N, Sudlow C, Downey P, Peakman T, Danesh J, Elliott P, *et al.* (2012): UK Biobank: Current status and what it means for epidemiology. Health Policy Technol 1:123–126.
26. Dutt RK, Hannon K, Easley TO, Griffis JC, Zhang W, Bijsterbosch JD (2022): Mental health in the UK Biobank: A roadmap to self-report measures and neuroimaging correlates. Hum Brain Mapp 43:816–832.
27. Alfaro-Almagro F, Jenkinson M, Bangerter NK, Andersson JLR, Griffanti L, Douaud G, *et al.* (2018): Image processing and quality control for the first 10,000 brain imaging datasets from UK Biobank. Neuroimage 166:400–424.
28. Pasternak O, Sochen N, Gur Y, Intrator N, Assaf Y (2009): Free water elimination and mapping from diffusion MRI. Magn Reson Med 62:717–730.
29. Zhang H, Schneider T, Wheeler-Kingshott CA, Alexander DC (2012): NODDI: Practical in vivo neurite orientation dispersion and density imaging of the human brain. Neuroimage 61:1000–1016.
30. Daducci A, Canales-Rodríguez EJ, Zhang H, Dyrby TB, Alexander DC, Thiran JP (2015): Accelerated Microstructure Imaging via Convex Optimization (AMICO) from diffusion MRI data. Neuroimage 105:32–44.
31. The University of Queensland Research Computing Centre (2024): Bunya Supercomputer. Brisbane: University of Queensland.
32. Renton AI, Dao TT, Johnstone T, Civier O, Sullivan RP, White DJ, *et al.* (2024): Neurodesk: An accessible, flexible and portable data analysis environment for reproducible neuroimaging. Nat Method 21:804–808.
33. Avants BB, Tustison NJ, Wu J, Cook PA, Gee JC (2011): An open source multivariate framework for n-tissue segmentation with evaluation on public data. Neuroinformatics 9:381–400.
34. NeuroImaging and Surgical Technologies Lab (2009): ICBM 152 nonlinear atlases. Available at: https://nist.mni.mcgill.ca/icbm-152-nonlinear-atlases-2009/. Accessed December 1, 2023.
35. Febo M, Perez PD, Ceballos-Diaz C, Colon-Perez LM, Zeng H, Ofori E, *et al.* (2020): Diffusion magnetic resonance imaging-derived free water detects neurodegenerative pattern induced by interferon-γ. Brain Struct Funct 225:427–439.
36. Uchida Y, Kan H, Sakurai K, Oishi K, Matsukawa N (2022): Quantitative susceptibility mapping as an imaging biomarker for Alzheimer's disease: The expectations and limitations. Front Neurosci 16:938092.
37. Zhang A, Leow A, Ajilore O, Lamar M, Yang S, Joseph J, *et al.* (2012): Quantitative tract-specific measures of uncinate and cingulum in major depression using diffusion tensor imaging. Neuropsychopharmacology 37:959–967.
38. Li BJ, Friston K, Mody M, Wang HN, Lu HB, Hu DW (2018): A brain network model for depression: From symptom understanding to disease intervention. CNS Neurosci Ther 24:1004–1019.
39. Yi SY, Barnett BR, Torres-Velázquez M, Zhang Y, Hurley SA, Rowley PA, *et al.* (2019): Detecting microglial density with quantitative multi-compartment diffusion MRI. Front Neurosci 13:81.
40. Bergamino M, Pasternak O, Farmer M, Shenton ME, Hamilton JP (2016): Applying a free-water correction to diffusion imaging data

uncovers stress-related neural pathology in depression. Neuroimage Clin 10:336–342.
41. Oestreich LKL, Lyall AE, Pasternak O, Kikinis Z, Newell DT, Savadjiev P, *et al.* (2017): Characterizing white matter changes in chronic schizophrenia: A free-water imaging multi-site study. Schizophr Res 189:153–161.
42. Pasternak O, Westin CF, Dahlben B, Bouix S, Kubicki M (2015): The extent of diffusion MRI markers of neuroinflammation and white matter deterioration in chronic schizophrenia. Schizophr Res 161:113–118.
43. Althubaity N (2023): Exploring brain CSF-mediated clearance in major depressive disorder using neuroimaging. Doctoral Thesis. London, United Kingdom: King's College.
44. Schubert JJ, Veronese M, Fryer TD, Manavaki R, Kitzbichler MG, Nettis MA, *et al.* (2021): A modest increase in 11C-PK11195-positron emission tomography TSPO binding in depression is not associated with serum C-reactive protein or body mass index. Biol Psychiatry Cogn Neurosci Neuroimaging 6:716–724.
45. Kamiya K, Hori M, Aoki S (2020): NODDI in clinical research. J Neurosci Methods 346:108908.
46. Dowell NG, Bouyagoub S, Tibble J, Voon V, Cercignani M, Harrison NA (2019): Interferon-alpha-induced changes in NODDI predispose to the development of fatigue. Neuroscience 403:111–117.
47. Ota M, Noda T, Sato N, Hidese S, Teraishi T, Setoyama S, *et al.* (2018): The use of diffusional kurtosis imaging and neurite orientation dispersion and density imaging of the brain in major depressive disorder. J Psychiatr Res 98:22–29.
48. Rajkowska G, Stockmeier CA (2013): Astrocyte pathology in major depressive disorder: Insights from human postmortem brain tissue. Curr Drug Targets 14:1225–1236.
49. Morris LS, Mehta M, Ahn C, Corniquel M, Verma G, Delman B, *et al.* (2022): Ventral tegmental area integrity measured with high-resolution 7-Tesla MRI relates to motivation across depression and anxiety diagnoses. Neuroimage 264:119704.
50. Marx W, Penninx BWJH, Solmi M, Furukawa TA, Firth J, Carvalho AF, Berk M (2023): Major depressive disorder. Nat Rev Dis Primers 9:44.
51. Derry HM, Padin AC, Kuo JL, Hughes S, Kiecolt-Glaser JK (2015): Sex differences in depression: Does inflammation play a role? Curr Psychiatry Rep 17:78.
52. Schachter J, Martel J, Lin CS, Chang CJ, Wu TR, Lu CC, *et al.* (2018): Effects of obesity on depression: A role for inflammation and the gut microbiota. Brain Behav Immun 69:1–8.
53. Luppino FS, de Wit LM, Bouvy PF, Stijnen T, Cuijpers P, Penninx BWJH, Zitman FG (2010): Overweight, obesity, and depression: A systematic review and meta-analysis of longitudinal studies. Arch Gen Psychiatry 67:220–229.
54. Burcusa SL, Iacono WG (2007): Risk for recurrence in depression. Clin Psychol Rev 27:959–985.
55. Dale AM, Fischl B, Sereno MI (1999): Cortical surface-based analysis. I. Segmentation and surface reconstruction. Neuroimage 9:179–194.
56. Fischl BFS (2012): FreeSurfer. Neuroimage 62:774–781.
57. Smith SM, Jenkinson M, Woolrich MW, Beckmann CF, Behrens TEJ, Johansen-Berg H, *et al.* (2004): Advances in functional and structural MR image analysis and implementation as FSL. Neuroimage 23 (suppl 1):S208–S219.
58. Jenkinson M, Beckmann CF, Behrens TEJ, Woolrich MW, Smith SM (2012): FSL. Neuroimage 62:782–790.
59. McCarthy P: FSLeyes (1.15.0). Zenodo. Available at: https://zenodo.org/records/15542963. Accessed July 15, 2025.
60. Tournier JD, Smith R, Raffelt D, Tabbara R, Dhollander T, Pietsch M, *et al.* (2019): MRtrix3: A fast, flexible and open software framework for medical image processing and visualisation. Neuroimage 202: 116137.
61. R Core Team (2022): R: A Language and Environment for Statistical Computing, Internet. Vienna, Austria: R Foundation for Statistical Computing.
62. Wickham H, François R, Henry L, Müller K: dplyr: A grammar of data manipulation. R package version 1.1.4. Available at: https://CRAN.R-project.org/package=dplyr. Accessed July 15, 2025.
63. Wickham H: ggplot2: Elegant graphics for data analysis. Available at: https://ggplot2.tidyverse.org. Accessed July 15, 2025.
64. Kassambara A (2023): ggpubr: 'ggplot2' based publication ready plots. R package version 0.6.0. Available at: https://CRAN.R-project.org/package=ggpubr. Accessed July 15, 2025.
65. McNamara A (2023): skimr: Compact and flexible summaries of data. R package version 2.1.5. Available at: https://CRAN.R-project.org/package=skimr. Accessed July 15, 2025.
66. Sievert C (2023): plotly: Create interactive web graphics via 'plotly.js'. R package version 4.10.1. Available at: https://CRAN.R-project.org/package=plotly. Accessed July 15, 2025.
67. Vaidyanathan R, Xie Y, Allaire JJ, Cheng J, Sievert C, Russel K, Hughes E, Posit Software (2023): PBC, htmlwidgets: HTML widgets for R. R package. Available at: https://CRAN.R-project.org/package=htmlwidgets, version 1.6.4. Accessed July 15, 2025.
68. Ho DE, Imai K, King G, Stuart EA (2023): MatchIt: Nonparametric preprocessing for parametric causal inference. R package version 4(0.0). Available at: https://CRAN.R-project.org/package=MatchIt. Accessed July 15, 2025.
69. Waddell K (2023): gghalves: Compose half-half plots using ggplot2. R package version 0.1.4. Available at: https://CRAN.R-project.org/package=gghalves. Accessed July 15, 2025.
70. Revelle W (2023): psych: Procedures for psychological, psychometric, and personality research. R package version 2(3.6). Available at: https://CRAN.R-project.org/package=psych. Accessed July 15, 2025.
71. Schloerke B, Crowley J, Cook D, Hofmann H, Wickham H (2023): GGally: Extension to ggplot2. R package version 2.1.2. Available at: https://CRAN.R-project.org/package=GGally. Accessed July 15, 2025.
72. Wickham H, Averick M, Bryan J, Chang W, D'Agostino McGowan L, François R, *et al.*: tidyverse: Easily install and load the 'Tidyverse'. R package. Available at: https://CRAN.R-project.org/package=tidyverse. Accessed July 15, 2025.
73. Fox J, Weisberg S (2023): car: Companion to applied regression. R package version 3:1–4. Available at: https://CRAN.R-project.org/package=car. Accessed July 15, 2025.
74. Zhu H (2023): kableExtra: Construct complex table with 'kable' and pipe syntax. R package version 1.3.5. Available at: https://CRAN.R-project.org/package=kableExtra. Accessed July 15, 2025.
75. Gohel D: officer: Manipulation of Microsoft Word and PowerPoint documents. R package version 0.6.2. Available at: https://CRAN.R-project.org/package=officer. Accessed July 15, 2025.
76. R Core Team (2023): tcltk: Tcl/Tk interface. R package version 4.3.1. Available at: https://CRAN.R-project.org/package=tcltk. Accessed July 15, 2025.
77. Wickham H, Seidel D (2023): scales: Scale functions for visualization. R package version 1.2.1. Available at: https://CRAN.R-project.org/package=scales. Accessed July 15, 2025.